Beitr. Phys. Atmosph., August 1989, p. 236–245
0005–8173/89/03 0236–10 $ 3.00/0


# Subgrid-Scale Fluxes and Flux Divergences in a Neutrally Stratified, Horizontally Inhomogeneous Surface-Layer

M. Claussen

Forschungszentrum Geesthacht, Postfach 1160, D-2054 Geesthacht, FRG

(Manuscript received December 1988; in revised form April and June 1989)

**Abstract**

Because of finite discretization in numerical models the flow is divided into the resolved part and the unresolved or subgrid-scale part. Transports due to subgrid-scale motions are partitioned as micro-turbulent fluxes, which are parameterized by assuming simple relationships between local fluxes and mean flow gradients valid for horizontally homogeneous flow, and meso-turbulent fluxes. In this study micro-turbulent and meso-turbulent fluxes of momentum and mass are computed for surface-layer flows over almost flat, but heterogeneous terrain by employing a micro-scale numerical model as a hypothetical grid box of a larger-scale model.

It has been found that micro-turbulent and meso-turbulent flux divergences are of the same order of magnitude in the case of shallow grid boxes. If the top of the grid box rises above the height up to which the mean flow can be modified by vertical turbulent diffusion, then the micro-turbulent flux divergences clearly dominate. For certain flow configurations, however, the horizontal diffusion by meso-turbulent motions can be an equally important diffusion term. For meso-turbulent and micro-turbulent mass transports similar results are found as for momentum.

**Zusammenfassung**

**Subskalige Flüsse und Flußdivergenzen in einer neutral geschichteten, horizontal inhomogenen Oberflächengrenzschicht**

Aufgrund der endlichen Diskretisierung in numerischen Modellen wird eine Strömung in einen vom Modell aufgelösten, skaligen und einen nicht aufgelösten, subskaligen Anteil aufgespalten. Die durch subskalige Bewegungsvorgänge induzierten Transporte werden wiederum aufgeteilt in mikroturbulente Flüsse, die durch für horizontal homogene Strömungen gültige Beziehungen zwischen lokalen Flüssen und lokalen mittleren Gradienten parameterisiert werden, sowie in mesoturbulente Flüsse. Die mikro- und mesoturbulenten Flüsse von Impuls und Masse wurden für bodennahe Strömungen über heterogenem, nahezu flachem Gelände berechnet, indem das Lösungsgebiet eines mikroskaligen Modells als Gittervolumen eines größerskaligen Modells angenommen wurde.

Die Berechnungen ergeben, daß die mikro- und mesoturbulenten Flußdivergenzen von gleicher Größenordnung sind, falls das größerskalige Gittervolumen hinreichend flach ist. Falls die vertikale Mächtigkeit des Gittervolumens die Höhe, bis zu der die mittlere Strömung durch die vertikale turbulente Diffusion noch beeinflußt werden kann, übersteigt, dann überwiegen die mikroturbulenten Flußdivergenzen, wobei in manchen Strömungen allerdings die Horizontaldiffusion durch Mesoturbulenz ein gleich wichtiger Diffusionsterm bleiben kann. Für die mikro- und mesoturbulenten Stofftransporte werden ähnliche Ergebnisse wie für den Impulstransport gefunden.

## 1 Introduction

Numerical models of atmospheric flow require parameterization of subgrid-scale transport, i.e. transport by motions which are not resolved by the grid. Current parameterization schemes of subgrid-scale transport within the atmospheric surface-lacer are based on similarity theories and scaling laws assuming that the surface-layer flow can be treated as a steady state, horizontally homogeneous flow which is in equilibrium with the underlying surface. However, with surface inhomogeneities, particularly at scales smaller than resolved by the grid of the model, these practical parameterization schemes are no longer applicable. In this case, it is necessary to consider grid averages of surface properties and of flow variables; also, the influence of local advection on the flow structure has to be regarded. Furthermore, it must be taken into account that subgrid-scale transport originates not only from micro-turbulent motions, but also from motions which are induced by heterogeneous terrain. These motions, which are referred to as 'meso-turbulent'

motions* in the following, may exhibit an energy spectrum different from micro-turbulence and do not necessarily follow the same similarity theories and scaling laws. (A more precise definition of meso-turbulence is given in Section 2.)

The partition of subgrid-scale motions as micro-turbulent and meso-turbulent is rather artificial. It is introduced because subgrid-scale motions are generally treated as micro-turbulence in current parameterization schemes. The questions, which are associated with this partition, are basically: How large is the meso-turbulent part of subgrid-scale transports in comparison with the micro-turbulent? Does the magnitude of meso-turbulent motions depend on the spatial distribution and on the height of roughness elements? Can transport by meso-turbulent motions be described in the same way as in the case of micro-turbulence, i.e. are similar relationships between local fluxes and local mean gradients still applicable? How do meso-turbulent motions affect the computation of spatially averaged micro-turbulent fluxes, particularly micro-turbulent fluxes at the earth's surface?

The latter question has recently been investigated by Mahrt (1987) and Claussen (1989). Mahrt (1987) has studied grid-averaged surface heat fluxes by assuming idealized spatial distributions of the Richardson number over a grid area. He found that the extra flux terms, which result from the spatial averaging of the relationship between turbulent flux and mean flow gradient, can be large. Neglect of these terms leads to an underestimation of heat transport in the stably stratified atmosphere. Claussen (1989) has used an effective drag coefficient and Stanton number for the calculation of area averages of surface fluxes in a neutrally stratified atmosphere. The effective drag coefficient and Stanton number are formulated such that the extra flux terms due to subgrid-scale correlations are taken into account implicitly.

In this study, the influence of transports due to meso-turbulent motion on the mean momentum and mass balance within the atmospheric surface-layer will be investigated. Attention is focused on a comparison of micro-turbulent and meso-turbulent fluxes as well as their divergences, i.e. basically on the first two questions being mentioned above. The meso-turbulent components of subgrid-scale motions are computed by use of a micro-scale model, which resolves the variation of surface-layer structure due to terrain inhomogeneities in detail, and by employing the entire flow domain of the micro-scale model (or parts of it) as one surface-layer grid box of a hypothetical larger-scale model.

The formal grid box averaging of the momentum and mass budget as well as the formal separation of subgrid-scale fluxes into micro- and meso-turbulent fluxes is developed in Section 2. In Section 3, numerical evaluations of these fluxes are discussed. The micro-scale model used for the numerical computations is briefly presented in Appendix A.

## 2 Formulation

The flow to be studied is a neutrally stratified, incompressible, inviscid turbulent flow in steady state. The flow is assumed to be homogeneous in one horizontal direction. The flow region is confined to the atmospheric surface-layer in which the influence of the earth's rotation on the flow is neglected. The basic equations of the mean flow are:

$$\frac{\partial \overline{U}}{\partial x} + \frac{\partial \overline{W}}{\partial z} = 0 \tag{1}$$

$$\overline{U}\frac{\partial \overline{U}}{\partial x} + \overline{W}\frac{\partial \overline{U}}{\partial z} + \frac{\partial \overline{U'U'}}{\partial x} + \frac{\partial \overline{U'W'}}{\partial z} = -\frac{1}{\rho_0}\frac{\partial \overline{P}}{\partial x} \tag{2a}$$

$$\overline{U}\frac{\partial \overline{W}}{\partial x} + \overline{W}\frac{\partial \overline{W}}{\partial z} + \frac{\partial \overline{U'W'}}{\partial x} + \frac{\partial \overline{W'W'}}{\partial z} = -\frac{1}{\rho_0}\frac{\partial \overline{P}}{\partial z} \tag{2b}$$

$$\overline{U}\frac{\partial \overline{C}}{\partial x} + \overline{W}\frac{\partial \overline{C}}{\partial z} + \frac{\partial \overline{U'C'}}{\partial x} + \frac{\partial \overline{W'C'}}{\partial z} = 0 \tag{3}$$

x and z are horizontal and vertical coordinates, $\overline{U}$ and $\overline{W}$ are the mean horizontal and vertical velocities, $\overline{C}$ is the mean concentration of a passive scalar, $U'$, $W'$, and $C'$ are the micro-turbulent perturbations, being defined as differences of actual and mean quantity, $\overline{U'W'}$, $\overline{U'U'}$, $\overline{W'W'}$, $\overline{U'C'}$, and $\overline{W'C'}$ are their covariances and autocovariances, so-called micro-turbulent fluxes, $\overline{P}$ is the mean hydrodynamic pressure, and $\rho_0$ is the density of the fluid. (The computation of micro-turbulent fluxes is discussed in Appendix A.). The above 'mean' quantities are defined as ensemble averages which have the properties that $\overline{\overline{U}\overline{U}} = \overline{U}\overline{U}$ and $\overline{\overline{U}U'} = 0$.

Because of finite discretization in numerical models the flow is divided into the resolved or grid-scale part and the unresolved or subgrid-scale part. Thus, any ensemble average is partitioned as

$$\overline{U}(x, y, z) = \{\overline{U}\} + \overline{U}^{+}(x, y, z) \tag{4}$$

where $\{\ldots\}$ symbolizes the volume-average over a grid box and the superscript '+' refers to a deviation from grid box average. $\overline{U}^{+}$ is called 'meso-turbulent' motion. It includes all motions on scales larger than the micro-turbulent scale (defined by the ensemble

* The expression 'meso-turbulence' is due to F. Wippermann and I. Bischoff-Gauss, Techn. Hochschule Darmstadt

average) and smaller than the scale resolved by the grid. In this study it is assumed that $\{\ldots\}$ refers to averages over fixed volumes. This 'control-volume' averaging has the same properties as ensemble averaging, in contrast to continuous volume averaging (Wyngaard, 1982), i.e. $\{\{\overline{U}\}\{\overline{U}\}\} = \{\overline{U}\}\{\overline{U}\}$ and $\{\{\overline{U}\}\overline{U}^+\} = 0$.

With the above partition in mind Eqs. (1)–(3) read

$$\frac{\partial\{\overline{U}\}}{\partial x} + \frac{\partial\{\overline{W}\}}{\partial z} = 0 \tag{5}$$

$$\{\overline{U}\}\frac{\partial\{\overline{U}\}}{\partial x} + \{\overline{W}\}\frac{\partial\{\overline{U}\}}{\partial z} + \left\{\frac{\partial\overline{U}^+\overline{U}^+}{\partial x}\right\} + \left\{\frac{\partial\overline{U}^+\overline{W}^+}{\partial z}\right\} + \left\{\frac{\partial\overline{U'U'}}{\partial x}\right\} + \left\{\frac{\partial\overline{U'W'}}{\partial z}\right\} = -\frac{1}{\rho_0}\frac{\partial\{\overline{P}\}}{\partial x} \tag{6a}$$

$$\{\overline{U}\}\frac{\partial\{\overline{W}\}}{\partial x} + \{\overline{W}\}\frac{\partial\{\overline{W}\}}{\partial z} + \left\{\frac{\partial\overline{U}^+\overline{W}^+}{\partial x}\right\} + \left\{\frac{\partial\overline{W}^+\overline{W}^+}{\partial z}\right\} + \left\{\frac{\partial\overline{U'W'}}{\partial x}\right\} + \left\{\frac{\partial\overline{W'W'}}{\partial z}\right\} = -\frac{1}{\rho_0}\frac{\partial\{\overline{P}\}}{\partial z} \tag{6b}$$

$$\{\overline{U}\}\frac{\partial\{\overline{C}\}}{\partial x} + \{\overline{W}\}\frac{\partial\{\overline{C}\}}{\partial z} + \left\{\frac{\partial\overline{U}^+\overline{C}^+}{\partial x}\right\} + \left\{\frac{\partial\overline{W}^+\overline{C}^+}{\partial z}\right\} + \left\{\frac{\partial\overline{U'C'}}{\partial x}\right\} + \left\{\frac{\partial\overline{W'C'}}{\partial z}\right\} = 0 \tag{7}$$

Implicit in Eq. (5) is the assumption that the incompressibility of the flow field is not only a local property, but is also preserved for spatial averages.

Considering the 'control-volume approach' in numerical modeling, only conservative quantities are formulated as averages over a grid volume, while transporting fluxes (advective and diffusive) are taken over the surfaces enveloping the grid volume, see Figure 1 (e.g. Anderson *et al.* 1984). Thus, the flux divergences due to meso-turbulent motions are:

$$\left\{\frac{\partial\overline{U}^+\overline{U}^+}{\partial x}\right\} = \frac{1}{\Delta X}\left(\langle\overline{U}^+\overline{U}^+\rangle_R - \langle\overline{U}^+\overline{U}^+\rangle_L\right) \tag{9a}$$

$$\left\{\frac{\partial\overline{U}^+\overline{W}^+}{\partial z}\right\} = \frac{1}{\Delta Z}\left([\overline{U}^+\overline{W}^+]_T - [\overline{U}^+\overline{W}^+]_B\right) \tag{9b}$$

$$\left\{\frac{\partial\overline{U}^+\overline{W}^+}{\partial x}\right\} = \frac{1}{\Delta X}\left(\langle\overline{U}^+\overline{W}^+\rangle_R - \langle\overline{U}^+\overline{W}^+\rangle_L\right) \tag{9c}$$

$$\left\{\frac{\partial\overline{W}^+\overline{W}^+}{\partial z}\right\} = \frac{1}{\Delta Z}\left([\overline{W}^+\overline{W}^+]_T - [\overline{W}^+\overline{W}^+]_B\right) \tag{9d}$$

$$\left\{\frac{\partial\overline{U}^+\overline{C}^+}{\partial x}\right\} = \frac{1}{\Delta X}\left(\langle\overline{U}^+\overline{C}^+\rangle_R - \langle\overline{U}^+\overline{C}^+\rangle_L\right) \tag{9e}$$

$$\left\{\frac{\partial\overline{W}^+\overline{C}^+}{\partial z}\right\} = \frac{1}{\Delta Z}\left([\overline{W}^+\overline{C}^+]_T - [\overline{W}^+\overline{C}^+]_B\right) \tag{9f}$$

where $\Delta Z$ and $\Delta X$ are the vertical and horizontal size of the large-scale grid box. $\langle\ldots\rangle_R$ indicates a vertical average over the 'right' or 'east' side of a grid box and $\langle\ldots\rangle_L$, over the 'left' or 'west' side; similarly, $[\ldots]_T$ refers to a horizontal average over the top side of a grid box and $[\ldots]_B$ over the bottom side which in this study is located at, or slightly above, the largest roughness length within the flow domain considered (see also Appendix A).

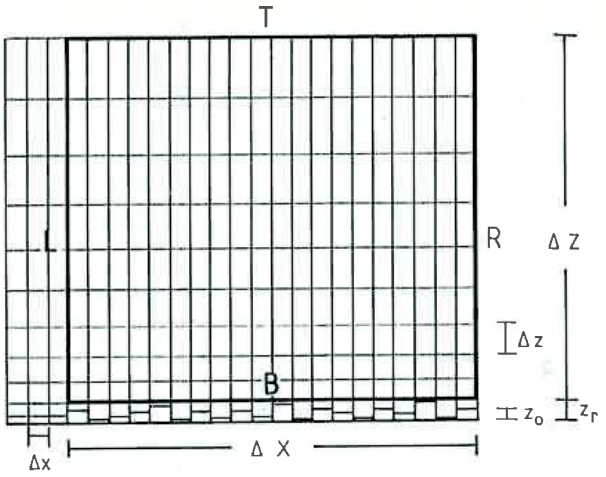


**Figure 1** Schematic sketch of a hypothetical grid box. The thin lines indicate the fine mesh of the micro-scale model within the large-scale grid box. The actual dimensions $\Delta X$, $\Delta Z$ of the large-scale grid box as well as $\Delta x$, $\Delta z$ of the fine mesh are given in the text (Section 3.1). $z_0$ is the roughness length and $z_r$ is the grid level at which the lower boundary condition is specified (see Appendix A).

All meso-turbulent fluxes but $\langle\overline{U}^+\overline{U}^+\rangle$ and $\langle\overline{U}^+\overline{C}^+\rangle$ vanish in a horizontally homogeneous flow. Since $\overline{U} = u_*/\kappa \ln(z/z_0)$ and $\overline{C} = c_*/\kappa \ln(z/z_{0c})$ in a neutral surface layer ($u_*$ is the friction velocity, $c_*$ is the turbulent concentration scale, $z_0$ is the roughness length for velocity, and $z_{0c}$ for concentration). $\langle\overline{U}^+\overline{U}^+\rangle$ and $\langle\overline{U}^+\overline{C}^+\rangle$ become

$$\langle\overline{U}^+\overline{U}^+\rangle = \frac{u_*^2}{\kappa^2} \tag{10a}$$

$$\langle\overline{U}^+\overline{C}^+\rangle = \frac{u_* c_*}{\kappa^2} \tag{10b}$$

provided that the height $z_T$ of the top surface of the large-scale grid box is much larger than $z_0$, the height of the bottom surface.

The same averaging procedure as above applies to the micro-turbulent fluxes. Since 'micro-turbulent fluxes are averaged over the grid box boundaries of a larger-scale model, fine-scale covariances are included in these averages, which the hypothesized larger-scale model does not see. This affects the relative size of the averaged micro-turbulent fluxes and complicates their parameterization in terms of larger-scale quantities. In this study, the influence of meso-turbulence on the (aver-

aged) micro-turbulent fluxes and flux divergences is not analyzed. Instead, attention is focused on the relative importance of meso-turbulent fluxes and flux divergences in comparison with averaged micro-turbulent fluxes and flux divergences.

## 3 Results

Because the numerical solution of the Eqs. (1)–(3) is quite expensive, only a few experiments have been performed in order to estimate the relative size of meso- and micro-turbulent fluxes and flux divergences as functions of magnitude and spatial distribution of roughness lengths. Two quite different spatial distribution of roughness lengths were considered as well as two configurations with large and small roughness lengths, respectively. Fortunately, the modification of mean flow and turbulence due to changes in surface roughness do not depend on the magnitude of the unperturbed horizontal mean velocity upstream of any roughness perturbation (e.g. Claussen, 1987). Therefore, the upstream velocity was held constant U = 1 m/s at z = 10 m for all experiments.

### 3.1 Momentum Advection

The following flow configurations are considered. The air flows from a homogeneous surface onto a surface with randomly varying surface roughness. Downstream of a fetch of 200 m of uniform surface roughness, the roughness length changes every 100 m. The entire flow domain in which the roughness length varies randomly is 5 km which is also the horizontal size of the hypothesized large-scale surface-layer grid box. The roughness lengths are taken from a positively skewed Weibull distribution with shape parameter a = 1.5 and scale parameter b = 0.06 (Case 1) and from two uniform roughness distributions (Case 2 and Case 3). The average roughness length is $[z_0] = 0.15$ m (Case 1 and Case 2) and $[z_0] = 0.005$ m (Case 3). The roughness length upstream of any roughness variation is specified $z_{00} = 0.11$ m (Case 1 and Case 2) and $z_{00} = 0.0032$ m (Case 3). These values are very close to the effective roughness lengths of the flow domain: $z_{oe} = 0.13$ m (Case 1), $z_{oe} = 0.12$ m (Case 2), $z_{oe} = 0.0035$ m (Case 3) (Mason, 1988; Claussen, 1989; see also Appendix B.). Hence, the difference between the upstream surface momentum flux and the average surface momentum flux is small. The average surface momentum flux exceeds its unperturbed value only by 3–4 %. Therefore, the above surface conditions can be considered nearly homogeneous on a large scale. The upstream friction velocity is $u_{*,0} = 0.09$ m/s for Cases 1 and 2, $u_{*,0} = 0.05$ m/s for Case 3.

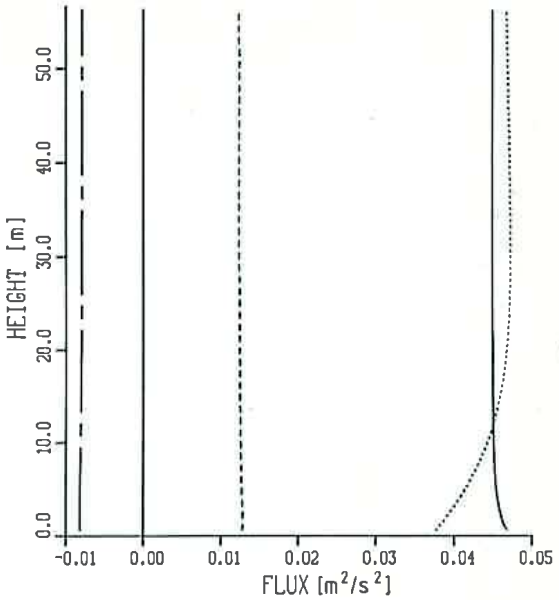


**Figure 2** Micro-turbulent fluxes [$m^2/s^2$] as function of the height [m] above ground of the top surface of the large-scale grid box. Flow configuration: Case 1 (see text). Full line: $\langle \overline{U'U'} \rangle_L$, horizontal flux of horizontal momentum through the upstream side; dotted line: $\langle \overline{U'U'} \rangle_R$, horizontal flux of horizontal momentum through the downstream side; dashed line: $[\overline{W'W'}]_T$, vertical flux of vertical momentum through the top side; chain-dashed line: $[\overline{U'W'}]_T$, vertical flux of horizontal momentum through the top side.

In order to get an idea of the relation between the large-scale grid box and the fine grid within it, the dimensions of the fine grid will be given: The vertical grid spacing depends on the maximum roughness length within the flow domain: $\Delta z = 0.02$ m for Case 3 and $\Delta z = 0.6$ m for Cases 1 and 2. The grid is stretched linearly by 5% from one grid box to the next as height increases. The maximum height of the entire flow domain measures 115 m. The horizontal grid spacing is kept constant at $\Delta x = 10$ m.

Figure 2 shows the micro-turbulent fluxes as function of the vertical depth of a hypothetical large-scale surface-layer grid box for Case 1. Since the fluxes vary slightly at larger heights, they are shown for the lowest 50 m only. The full line refers to the horizontal flux of horizontal momentum $\langle \overline{U'U'} \rangle_L$ through the upstream side, the dotted line to $\langle \overline{U'U'} \rangle_R$, i.e. the same flux through the downstream side of the hypothetical grid box. Both fluxes are much larger than the vertical flux of vertical momentum $[\overline{W'W'}]_T$ (dashed line) through the top side of the grid box. Due to upstream effects, $\langle \overline{U'U'} \rangle_L$ is not constant with height. $\langle \overline{U'U'} \rangle_R$ depends on the (random) roughness length at the downstream edge of the large-scale grid box, but it is also influenced by the roughness lengths farther upstream because the upstream roughness lengths have already modified mean flow and

turbulence. At larger heights, in this case at $z \geqslant 10$m approximately, $\langle \overline{U'U'} \rangle_R$ should be exclusively determined by the upstream roughness lengths. The vertical transport of horizontal momentum $[\overline{U'W'}]_T$ (chain-dashed line) through the top of the grid box is almost as large as $[\overline{W'W'}]_T$, but it is directed downward, towards the surface. The other fluxes $\langle \overline{U'W'} \rangle_R$ and $\langle \overline{U'W'} \rangle_L$ are as large as $[\overline{U'W'}]_T$ and of same sign. They are not shown in Figure 2.

In Figure 3, the meso-turbulent fluxes are depicted for Case 1. As for the micro-turbulent fluxes, the horizontal fluxes of horizontal momentum $\langle \overline{U}^+\overline{U}^+ \rangle_R$ (dotted line) and $\langle \overline{U}^+\overline{U}^+ \rangle_L$ (full line) are much larger than the other fluxes which are hardly noticeable at that scale. Notice that both, $\langle \overline{U}^+\overline{U}^+ \rangle_R$ and $\langle \overline{U}^+\overline{U}^+ \rangle_L$, approach the value $u_{*,0}^2/\kappa^2 \simeq 0.05$ with increasing thickness of the large-scale grid box. In contrast to its micro-turbulent counterpart, the vertical flux of horizontal momentum, $[\overline{U}^+\overline{W}^+]_T$, can be positive and negative; however, this effect is negligibly small and, therefore, cannot be seen in Figure 3.

The micro- and meso-turbulent fluxes in the Case 2 are similar to the fluxes in the Case 1 concerning their vertical structure as well as their magnitude. Even in the Case 3, they exhibit a similar behavior, except that the meso-turbulent fluxes are smaller than in the Case 1 by a factor of 2, the micro-turbulent fluxes by a factor of 3. Because of this similarity, the fluxes of Cases 2 and 3 are not shown.

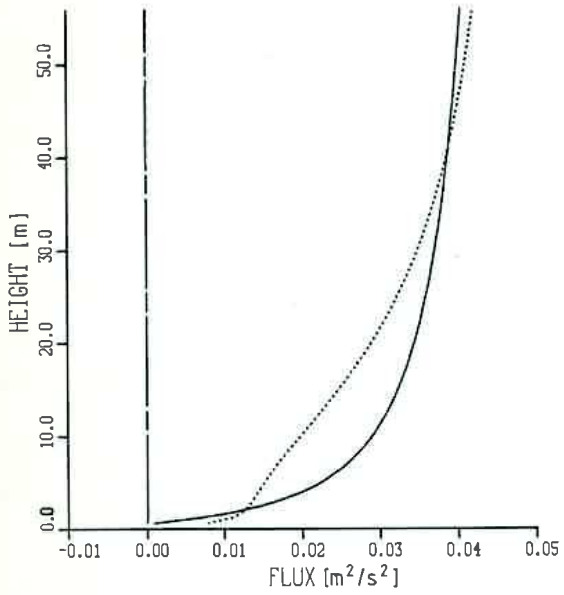


**Figure 3** Meso-turbulent fluxes $[m^2/s^2]$ as function of the height [m] above ground of the top surface of the large-scale grid box. Flow configuration: Case 1. Full line: $\langle \overline{U}^+\overline{U}^+ \rangle_L$, horizontal flux of horizontal momentum through the upstream side; dotted line: $\langle \overline{U}^+\overline{U}^+ \rangle_R$, horizontal flux of horizontal momentum through the downstream side; chain-dashed line: $[\overline{U}^+\overline{W}^+]_T$, vertical flux of horizontal momentum through the top side.

Considering the momentum budget, the flux divergences are much more interesting than the fluxes themselves. In Figures 4 and 5, the micro-turbulent flux divergences are shown for Cases 1 and 2, respectively. The vertical diffusion of horizontal and vertical momentum $\left\{\frac{\partial \overline{U'W'}}{\partial z}\right\}$ (dashed line) and $\left\{\frac{\partial \overline{W'W'}}{\partial z}\right\}$ (chain-dotted line), respectively, are the largest terms. The

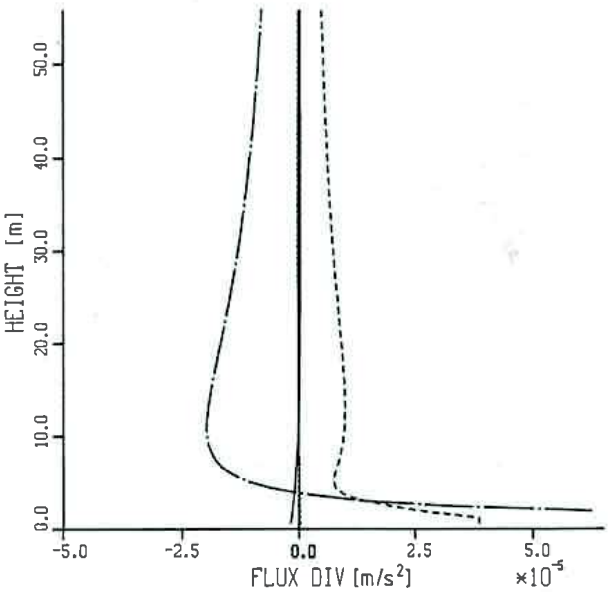


**Figure 4** Micro-turbulent flux divergence $[m/s^2]$ as function of the height [m] above ground of the top surface of the large-scale grid box. Flow configuration: Case 1. Full line: $\left\{\frac{\partial \overline{U'U'}}{\partial x}\right\}$, dotted line: $\left\{\frac{\partial \overline{U'W'}}{\partial x}\right\}$, dashed line: $\left\{\frac{\partial \overline{U'W'}}{\partial z}\right\}$, and chain-dotted line: $\left\{\frac{\partial \overline{W'W'}}{\partial z}\right\}$.

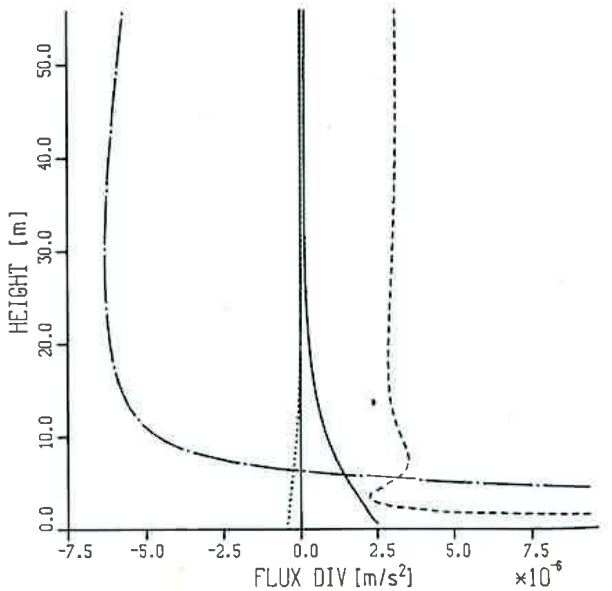


**Figure 5** Same as Figure 4, except for flow configuration Case 2 (see text).

horizontal diffusion terms $\left\{\frac{\partial \overline{U'U'}}{\partial x}\right\}$, full line and $\left\{\frac{\partial \overline{U'W'}}{\partial x}\right\}$, dotted line are small terms.

The meso-turbulent flux divergences $\left\{\frac{\partial \overline{U}^+\overline{W}^+}{\partial z}\right\}$, $\left\{\frac{\partial \overline{W}^+\overline{W}^+}{\partial z}\right\}$, and $\left\{\frac{\partial \overline{U}^+\overline{U}^+}{\partial x}\right\}$ seem to be of the same order of magnitude in both cases (see Figures 6 and 7). For Case 3 the micro- and meso-turbulent flux divergences are not shown. They look similar to those in the Case 2, but they are smaller by factor of 4 approximately.

Comparing micro-turbulent and meso-turbulent flux divergences, it is seen that for a shallow grid box both types of subgrid-scale flux divergences can be equally important diffusion terms. For deeper grid boxes the micro-turbulent flux divergences dominate.

The vertical depth $\Delta Z$ of a surface-layer grid box should be $\Delta Z \sim O(z_d)$ in order to neglect the meso-turbulent diffusion terms. $z_d$ is the so-called diffusion height which forms a scale for the height up to which the mean flow can be modified by vertical turbulent diffusion. $z_d$ is approximately given by $z_d = 0.7[z_0](L_c/[z_0])^{4/5}$ where $L_c$ is the wavelength of variations of surface roughness and $[z_0]$ is the average roughness length (Claussen, 1989; see also Appendix B). For Cases 1 and 2, $z_d \simeq 60$m. From Figures 6 and 7, it can be inferred that $\Delta Z \geqslant 30$m is quite sufficient a condition for the neglection of meso-turbulent diffusion terms.

By comparing Figures 5 and 7, it can be seen that in this case the meso-turbulent horizontal diffusion $\left\{\frac{\partial \overline{U}^+\overline{U}^+}{\partial x}\right\}$ is a small, but not negligibly small term in comparison with other micro-turbulent diffusion terms, even for a deep grid box. The term $\left\{\frac{\partial \overline{U'W'}}{\partial z}\right\}$ is only by a factor of 2–3 larger than $\left\{\frac{\partial \overline{U}^+\overline{U}^+}{\partial x}\right\}$. Similar is found in the Case 3 in which $\left\{\frac{\partial \overline{U'W'}}{\partial z}\right\} \sim 4\left\{\frac{\partial \overline{U}^+\overline{U}^+}{\partial x}\right\}$. By contrast, in the Case 1, $\left\{\frac{\partial \overline{U'W'}}{\partial z}\right\}$ exceeds $\left\{\frac{\partial \overline{U}^+\overline{U}^+}{\partial x}\right\}$ by a factor of 20 approximately. In the Cases 2 and 3, $\left\{\frac{\partial \overline{U}^+\overline{U}^+}{\partial x}\right\}$ happens to have the same sign as $\left\{\frac{\partial \overline{U'U'}}{\partial x}\right\}$.

In order to get an idea of the relative importance of meso-turbulent and micro-turbulent flux divergences in the cases of a large-scale change in surface roughness, the upstream roughness length $z_{00}$ has been altered to $z_{00} = 0.01$m for Case 3. Although the change in surface roughness from $z_{00} = 0.01$m to $z_{oe} = 0.0035$m is not a large one, the micro-turbulent flux divergences have been found to increase by an order of magnitude, while the meso-turbulent flux divergences increased only slightly.

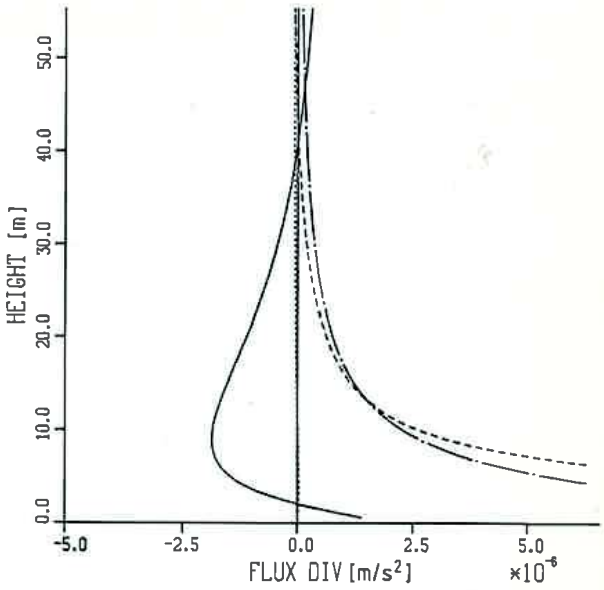


**Figure 6** Meso-turbulent flux divergence [m/s²] as function of the height [m] above ground of the top surface of the large-scale grid box. Flow configuration: Case 1. Full line: $\left\{\frac{\partial \overline{U}^+\overline{U}^+}{\partial x}\right\}$, dotted line: $\left\{\frac{\partial \overline{U}^+\overline{W}^+}{\partial x}\right\}$, dashed line: $\left\{\frac{\partial \overline{U}^+\overline{W}^+}{\partial z}\right\}$, and chain-dotted line: $\left\{\frac{\partial \overline{W}^+\overline{W}^+}{\partial z}\right\}$.

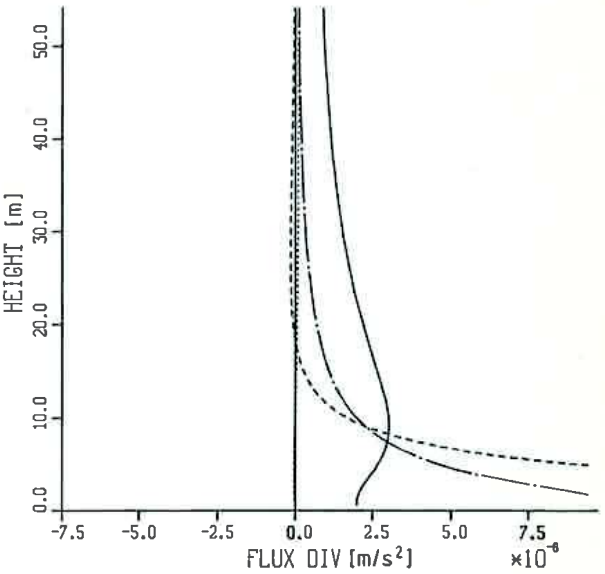


**Figure 7** Same as Figure 6, except for flow configuration Case 2 (see text).

Flows over strips of modified roughness have been simulated, but were not systematically analyzed. Therefore, the results are not presented. These results agree qualitatively with the above-mentioned in this sense that micro-turbulent flux divergences were found to exceed meso-turbulent flux divergences for sufficiently thick large-scale grid boxes. Only the meso-turbulent horizontal diffusion $\left\{\frac{\partial \overline{U}^+\overline{U}^+}{\partial x}\right\}$ was

not negligibly small in comparison with $\left\{\frac{\partial \overline{U'W'}}{\partial z}\right\}$ provided that the strip of modified roughness covers a large portion of the (large-scale) grid box.

### 3.2 Mass Advection

In order to evaluate the meso- and micro-turbulent flux divergences in Eq. (7), a flow configuration is considered which is the same as for Case 1 in the previous section. In addition, the roughness lengths $z_{0c}$ of concentration are specified such that $\ln(z_0/z_{0c}) = 2.3$ (see also Appendix A).

The structure of micro-turbulent and meso-turbulent concentration fluxes resembles the structure of momentum fluxes; therefore, only the more interesting flux divergences are shown. The full line in Figure 8 refers to the vertical divergence of the micro-turbulent vertical flux $\left\{\frac{\partial \overline{W'C'}}{\partial z}\right\}$, the dotted line to the meso-turbulent $\left\{\frac{\partial \overline{W}^+\overline{C}^+}{\partial z}\right\}$, and the dashed line to the horizontal divergence of the meso-turbulent horizontal flux $\left\{\frac{\partial \overline{U}^+\overline{C}^+}{\partial x}\right\}$. The term $\left\{\frac{\partial \overline{U'C'}}{\partial x}\right\}$ is not shown, because it is at least one order of magnitude smaller than $\left\{\frac{\partial \overline{W'C'}}{\partial z}\right\}$. For shallow grid boxes, meso-turbulent and micro-turbulent flux divergences are equally important terms in the mass budget. However, as the grid box gets deeper, the micro-turbulent flux divergence $\left\{\frac{\partial \overline{W'C'}}{\partial z}\right\}$ becomes the dominant term, $\left\{\frac{\partial \overline{U}^+\overline{C}^+}{\partial x}\right\}$ is the second largest, but negligibly small in comparison with $\left\{\frac{\partial \overline{W'C'}}{\partial z}\right\}$.

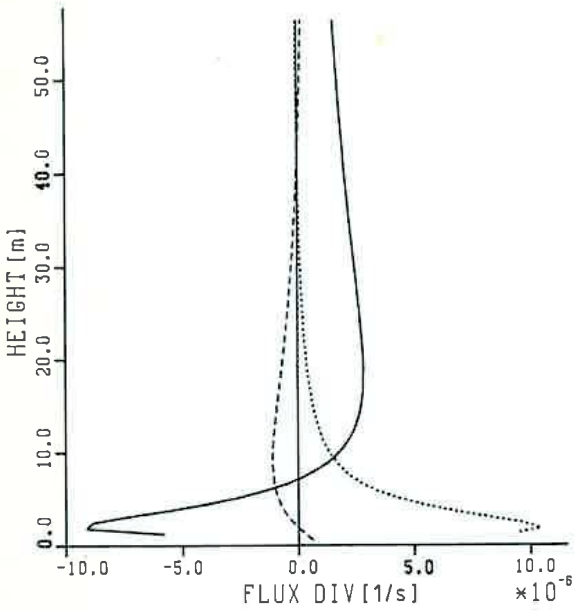


**Figure 8** Meso- and micro-turbulent flux divergence [1/s] of the concentration of a passive contaminant as function of the height [m] above ground of the top surface of the large-scale grid box. Full line: $\left\{\frac{\partial \overline{W'C'}}{\partial z}\right\}$, dotted line: $\left\{\frac{\partial \overline{W}^+\overline{C}^+}{\partial z}\right\}$, dashed line: $\left\{\frac{\partial \overline{U}^+\overline{C}^+}{\partial x}\right\}$.

If the same flow configuration is considered, but with the surface resistance (see Appendix A) changed, then $\left\{\frac{\partial \overline{W'C'}}{\partial z}\right\}$ was found to be by far the largest term of meso- and micro-turbulent flux divergences. However, this result has to be considered as preliminary, because the surface resistance was assumed to be a 'material constant', whereas in nature the surface resistance should depend on the specific admixture as well as on other environmental variables.

## 4 Conclusion and Discussion

Because of finite discretization in numerical models the flow is divided into the resolved part and the unresolved or subgrid-scale part. Transports due to subgrid-scale motions are (artificially) partitioned as micro-turbulent fluxes, which are parameterized by assuming simple relationships between local fluxes and mean flow gradients valid for horizontally homogeneous flow, and meso-turbulent fluxes. Meso-turbulence includes all motions on scales larger than the micro-turbulent scale and smaller than the scale resolved by the grid. It is shown that all meso-turbulent fluxes except the horizontal transport of horizontal momentum and concentration vanish in a horizontally homogeneous surface layer.

Micro-turbulent and meso-turbulent fluxes of momentum and mass are computed for surface-layer flows over almost flat, but heterogeneous terrain. The micro-turbulent fluxes are calculated by a fine-mesh model and then averaged over the boundaries of a hypothetical large-scale grid box. Thus, these averages are affected by meso-turbulence and, therefore, averaged micro-turbulent and meso-turbulent fluxes are not completely independent quantities. The influence of meso-turbulence on averaged micro-turbulence, which certainly complicates parameterization of averaged micro-turbulent fluxes in terms of larger-scale quantities, has not been investigated in this study. This problem will be addressed in a forthcoming paper (Claussen, 1989). Here, only the relative importance of terms which emerge from grid box averaging and which differ from the (averaged) micro-turbulent terms have been estimated.

The following results have been found. Meso-turbulent and micro-turbulent horizontal fluxes are the largest. Considering the vertical fluxes, the meso-turbulent

transports are negligibly small in comparison with micro-turbulent transports. A peculiar behavior is noticed for the vertical transport of horizontal momentum. In contrast to the micro-turbulent flux, the meso-turbulent flux can be directed away from the earth's surface as well as towards it. However, this effect is very small.

The divergences of vertical transport (vertical diffusion) of vertical and horizontal momentum are the largest micro-turbulent terms. The same is true for the meso-turbulent flux divergences, except that also the horizontal diffusion of horizontal momentum becomes important. Both micro-turbulent and meso-turbulent flux divergences are of the same order of magnitude in the case of shallow grid boxes. If the top of the grid box rises above the height up to which the mean flow can be modified by vertical turbulent diffusion, then the micro-turbulent flux divergences clearly dominate. Only the horizontal meso-turbulent diffusion of horizontal momentum may still be important.

The magnitude of meso-turbulent and micro-turbulent flux divergences depends on the magnitude of the roughness lengths (compare Cases 2 and 3). The relative importance of meso-turbulent flux divergences in comparison with micro-turbulent flux divergences seems to be a function of the spatial distribution of roughness lengths (see Cases 1 and 2). If the roughness lengths follow a positively skewed Weibull distribution, then meso-turbulent flux divergences can be neglected for a sufficiently thick (surface-layer) grid box; for uniformly distributed roughness lengths, the horizontal meso-turbulent diffusion becomes an important term. Since this meso-turbulent divergence has the same sign as its much smaller micro-turbulent counterpart, it can be interpreted as an additional horizontal diffusion. Perhaps, one could, therefore, simply use the same parameterization as for micro-turbulent horizontal diffusion, but with an enhanced diffusion coefficient. The parameterization of horizontal diffusion is, however, quite problematic. It should depend on the advection scheme of a numerical model itself, because many models already use some kind of artificial horizontal diffusion for reasons of numerical stability. At this point a word of caution is necessary. The micro-turbulence is parameterized as three-dimensional turbulence, i.e. energy is fed from the mean flow into all turbulent velocity components (see Appendix A). The mean flow is, however, two-dimensional. Therefore, the perturbation of mean flow, i.e. the meso-turbulence, could resemble two-dimensional rather than three-dimensional turbulence. Thus, before thinking of a parameterization of meso-turbulent horizontal diffusion, it should be investigated whether a flow with imbedded three-dimensional surface inhomogeneities yields results similar to the above-mentioned.

For meso-turbulent and micro-turbulent mass fluxes and flux divergences similar results are found as for momentum fluxes. It has been mentioned that changes in surface resistance strongly influence the modification of passive scalars. Therefore, further research has to focus on the dependence of meso-turbulence and (averaged) micro-turbulence on the variation of surface resistances.

## Appendix

### A. The Numerical Model

The numerical model which is used to simulate the surface-layer flow over flat, but inhomogeneous terrain is described in detail in Claussen (1987, 1988, 1989). The basic equations of the model are Eqs. (5)–(7). The meso-turbulent transports are neglected, since the model resolves surface inhomogeneities; thus, there are no subgrid-scale variations of surface conditions.

Turbulent momentum fluxes are calculated by using a modified Boussinesq approach:

$$-\overline{U_i' U_j'} = K_m \left( \frac{\partial \overline{U}_i}{\partial x_j} + \frac{\partial \overline{U}_j}{\partial x_i} \right) - c_i \overline{E} \delta_{ij}. \qquad \text{(A1)}$$

$\overline{E}$ is the turbulent kinetic energy:

$$\overline{E} = \frac{1}{2} \overline{U_i' U_i'}.$$

(In Eq. (A1), Cartesian tensor notation and the Einstein summation convention are used. Subscript '1' refers to the x-component and subscript '2' to the z-component of a vector.) The original Boussinesq approach (see Hinze, 1975) uses $c_{1,2} = 2/3$. Hence, $c_1 = 1.042$ and $c_2 = 0.285$ is chosen, because it is observed that the variance of horizontal velocity fluctuations is larger than that of vertical velocity fluctuations. The values $c_{1,2}$ which are valid for homogeneous terrain are taken from Panofsky and Dutton (1984). The use of the original or the modified Boussinesq model only marginally alters the results of numerical simulations of local advection processes; however, the difference is important considering the interpretation of variances themselves.

The turbulent fluxes of passive constituents are parameterized by

$$-\overline{U_i' C'} = \alpha_c K_m \left( \frac{\partial \overline{C}}{\partial x_i} \right) \qquad \text{(A2)}$$

where $\alpha_c$ is the inverse turbulent Schmidt number. Since in this study no particular tracer is considered, $\alpha_c = 1$ is chosen.

For the exchange coefficient $K_m$ the so called $E-\epsilon$ (also known as $k-\epsilon$) model is used, hence

$$K_m = c_0^4 \frac{\overline{E}^2}{\overline{\epsilon}} \tag{A3}$$

where $\epsilon$ is the dissipation of turbulent kinetic energy. In contrast to other first-order turbulence closures, the $E-\epsilon$ model realistically simulates a slow relaxation of eddy viscosity to varying surface conditions (Claussen, 1988). Considering the deviation of the surface-layer flow from local equilibrium, the $E-\epsilon$ model yields results similar to that of a second-order closure model, but it is less complicated to handle.

In this model the earth's rotation is neglected which might pose a problem under certain circumstances. Coriolis forces affect atmospheric surface-layer flow at heights larger than a few decameters not because the forces themselves produce a significant effect on the flow modification in this range, but because the vertical turbulent diffusion is bounded (see Taylor, 1969). In an infinitely extended, neutral surface-layer, as assumed in this study, the turbulent exchange coefficient increases linearly with height, whereas in the planetary boundary-layer it attains a maximum value at a certain height above which it decreases. Thus, this model uses an unrealistically strong diffusion coefficient at heights larger than a few decameters which implies that the predicted flow modification becomes larger than realistic as height increases above a few decameters.

Equations (5)–(7) are solved by using a stream function-vorticity model. Details of the numerical model including specification of constants are given in Claussen (1987, 1988).

The boundary conditions for Eqs. (5) and (6) are discussed in detail by Claussen (1987, 1988) and for Eq. (7) by Claussen (1989). Here, the boundary conditions will be presented only briefly.

The lower boundary condition is specified at some height $z = z_r$ at or slightly above the largest roughness length within the flow domain. Varying surface elevation is not taken into account. At $z = z_r$ the flow is assumed to be in equilibrium with its local roughness and surface resistance. Hence,

$$\overline{C}(z_r) = \frac{c_*}{\kappa} \ln\left(\frac{z_r}{z_{0c}}\right) + c_* u_* r_s \tag{A4}$$

where $u_*$ is the friction velocity, $c_*$ is the turbulent concentration scale, and $r_s$ is the surface resistance which is a measure for the resistance against transport of an admixture into a surface. In this study, $r_s$ is an arbitrarily chosen, positive constant. $z_{0c}$ is the so-called roughness length for concentration. The numerical value of $z_{0c}$ depends on the pollutant as well as the surface characteristics. Over surfaces covered with a vegetation or with similar porous or fibrous roughness elements, $\ln(z_0/z_{0c})$ is approximately a constant $\simeq 2.3$ (e.g. Hicks, 1985).

As upstream condition it is assumed that the entire boundary-layer is in equilibrium with the underlying surface. The dimensions of the flow domain are chosen such that the upper boundary is at least twice as deep as any internal boundary-layer of velocity or concentration. Thus, it seems warranted to use the unperturbed upstream values as upper boundary values.

### B. The Effective Roughness Length

Recently, various studies have addressed the parameterization of turbulent momentum transfer over heterogeneous terrain with emphasis on the formulation of an 'effective' roughness length (see Mason, 1988). Although there is no generally valid definition of an effective roughness length, it is agreed that the effective roughness length is a value intended to represent a spatial average over heterogeneous terrain such that by use of boundary-layer similarity theory a correct spatial average of surface stress or mean velocity is found.

Wieringa (1986) and Mason (1988) suggest evaluation of an effective roughness length $z_{0e}$ by averaging surface momentum fluxes based on a so-called 'blending' height $z_b$. Mason (1988) considers the blending height a scale-height at which the flow is approximately in equilibrium with the local surface and also independent of position. He finds $z_{0e}$ from

$$\frac{1}{\left(\ln \frac{z_b}{z_{0e}}\right)^2} = \frac{1}{\left(\ln \frac{z_b}{z_0}\right)^2} . \tag{B1}$$

Furthermore, Mason (1988) provides a heuristic model which indicates that roughly $z_b/L_c \sim o(10^{-2})$ where $L_c$ is the horizontal scale or wave length of roughness variations. Claussen (1989) argues that the magnitude of $z_b$ should be larger than given by Mason (1988) and it should be of the same order as $z_d$, the diffusion height. He also shows that the surface momentum flux is calculated sufficiently accurate, if $z_{0e}$ is determined by

$$\frac{1}{\ln \frac{z_d}{z_{0e}}} = \frac{1}{\ln \frac{z_d}{z_0}} . \tag{B2}$$

The latter estimate of $z_{0e}$ is used in this study.

## Acknowledgements

The author wishes to thank Prof. H. Grassl, Universität Hamburg, and Dr. D. Eppel, Forschungszentrum Geesthacht, for discussion. The constructive critique of the anonymous referees is also acknowledged.

## References

*Anderson, D. A., J. C. Tannehill*, and *R. H. Pletcher*, 1984: Computational fluid mechanics and heat transfer. McGraw Hill Book Company, New York, 599 p.

*Claussen, M.*, 1987: The flow in a turbulent boundary layer upstream of a change in surface roughness. Boundary-Layer Meteorol., **40**, 31–86.

*Claussen, M.*, 1988: Models of eddy viscosity for numerical simulation of horizontally inhomogeneous surface layer flow. Boundary-Layer Meteorol., **42**, 337–369.

*Claussen, M.*, 1989: Area-averaging of surface fluxes in a neutrally stratified, horizontally inhomogeneous atmospheric boundary layer. Accepted in Atmos. Environ.

*Hicks, B. B.*, 1985: Application of forest-atmosphere turbulent exchange information. In: B. A. Hutchison and B. B. Hicks (eds.), The Forest-Atmosphere Interaction, 631–644.

*Hinze, H. O.*, 1975: Turbulence McGraw-Hill Book Comp., New York, 790 p.

*Mahrt, L.*, 1987: Grid-averaged surface fluxes. Mon. Wea. Rev., **15**, 1550–1560.

*Mason, P. L.*, 1988: The formation of areally-averaged roughness lengths. Quart. J. R. Met. Soc., **114**, 399–420.

*Panofsky, H. A.* and *J. A. Dutton*, 1984: Atmospheric turbulence. Wiley-Interscience publ., 397 p.

*Taylor, P. A.*, 1969: The planetary boundary layer above a change in surface roughness. J. Atmos. Sci., **26**, 432–440.

*Wieringa, J.*, 1986: Roughness-dependent geographical interpolation of surface wind speed averages. Quart. J. R. Met. Soc., **112**, 867–889.

*Wyngaard, J. C.*, 1982: Boundary-layer modeling. In: Nieuwstadt, F. T. M. and VanDop, H. (eds.), Atmospheric turbulence and air pollution modelling, 69–107.